mathematics

Article

Local and Parallel Stabilized Finite Element Methods Based on the Lowest Equal-Order Elements for the Stokes–Darcy Model

Jing Han and Guangzhi Du *

School of Mathematics and Statistics, Shandong Normal University, Jinan 250014, China; jinghan@sdnu.edu.cn
* Correspondence: gzdu@sdnu.edu.cn

Abstract: In this article, two kinds of local and parallel stabilized finite element methods based upon two grid discretizations are proposed and investigated for the Stokes–Darcy model. The lowest equal-order finite element pairs ($\mathbf{P}_1$-P_1-P_1) are taken into account to approximate the velocity, pressure, and piezometric head, respectively. To circumvent the inf-sup condition, the stabilized term is chosen as the difference between a consistent and an under-integrated mass matrix. The proposed algorithms consist of approximating the low-frequency component on the global coarse grid and the high-frequency component on the local fine grid and assembling them to obtain the final approximation. To obtain a global continuous solution, the technique tool of the partition of unity is used. A rigorous theoretical analysis for the algorithms was conducted and numerical experiments were carried out to indicate the validity and efficiency of the algorithms.

Keywords: Stokes–Darcy model; stabilized finite element method; local and parallel finite element method; partition of unity

MSC: 65N15; 65N30; 65N55

check for updates

Citation: Han, J.; Du, G. Local and Parallel Stabilized Finite Element Methods Based on the Lowest Equal-Order Elements for the Stokes–Darcy Model. *Mathematics* **2023**, *11*, 4820. https://doi.org/10.3390/math11234820

Academic Editor: Vasily Novozhilov

Received: 19 October 2023
Revised: 19 November 2023
Accepted: 28 November 2023
Published: 29 November 2023

Copyright: © 2023 by the authors. Licensee MDPI, Basel, Switzerland. This article is an open access article distributed under the terms and conditions of the Creative Commons Attribution (CC BY) license (https://creativecommons.org/licenses/by/4.0/).

1. Introduction

The Stokes–Darcy system describes a model that is composed of the Stokes equations for the fluid flow and Darcy's law for the porous media flow with coupled interface conditions. The finite element method is widely used for solving this model since it is more applicable to the complex region and its numerical analysis is perfect. Until now, there have been lots of works on this coupled model, for instance, coupled finite element methods [1–3], two-grid methods [4–6], multi-grid methods [7], domain decomposition methods [8–11], and so on. Compared with coupled methods, decoupled methods could save a lot of computing time by dividing the coupled problem into two sub-problems. Among these decoupled methods, the local and parallel finite element methods were first proposed by Xu and Zhou to solve the elliptic boundary value problems by combining the two-grid method and domain decomposition technique in [12,13]. Subsequently, many researchers generalized them to the Stokes problem [14], the Navier–Stokes problem [15–17], the Stokes–Darcy model [18], the Navier–Stokes–Darcy model [19], and the MHD problem [20].

In this paper, the local and parallel finite element methods are considered to solve the coupled problem. The steps of the local and parallel finite element method can be presented as follows. Firstly, the Stokes–Darcy model is approximated to obtain the numerical solution by using standard finite element method on a coarse grid. Secondly, the coupled problem is decoupled into two individual sub-problems and the complete domain is divided into a series of sub-domains. Then, the residual problems are solved on a fine grid in these sub-domains. To avoid the effect of the artificial Dirichlet boundary condition, each sub-domain is properly enlarged to a larger domain. Finally, the numerical solution is assembled on the coarse grid and the residual together. However, the solution for the Stokes–Darcy model using local and parallel finite element methods can be improved since the solutions are, in general, globally discontinuous. To overcome this drawback, the most popular idea is to introduce the partition of unity technique, which is adaptable and controllable, to decompose the computational domain [21,22].

It is well known that finite element spaces utilized for the coupled Stokes–Darcy model should satisfy the inf-sup (or LBB) condition. Although the lowest equal-order finite element pairs do not satisfy the inf-sup condition, they are computationally convenient in practical applications because of the identical degree distribution for the velocity and pressure. Therefore, the lowest equal-order finite element pairs have attracted much more attention in recent years. To circumvent the inf-sup condition, many stabilized techniques have been researched, such as local pressure projection stabilized methods [23–25] and the stabilized methods based on two local Gauss integrations [26–30]. Among these stabilized methods, the stabilized method based on two local Gauss integrations does not need to calculate high-order derivatives and construct the projection operator; however, it can be computed at the element level.

In this paper, two parallelized stabilized finite element algorithms are proposed and analyzed for the mixed Stokes–Darcy model by combining the classical local and parallel finite element methods and the stabilized method based on two local Gauss integration techniques. Compared to our previous work, for instance [18], the lowest equal-order finite element pairs are considered. The algorithms in this study and those in [18] were devised with the understanding that, for a solution to the mixed problem, the low-frequency components have the global property while the high-frequency components have the local property. Hence, the low-frequency components are computed on a coarse mesh and the high-frequency components are obtained on a fine mesh by some local and parallel procedures. The theoretical results indicate that our methods could derive the same error convergence orders as the parallel methods provided in [18]. On the other hand, the numerical results show that algorithms in this study could achieve a better error accuracy and take less time compared with the parallel methods provided in [18].

The rest of this article is organized as follows. In Section 2, the Stokes–Darcy model is introduced. The finite element spaces and some useful notations are described in Section 3. In Section 4, two local and parallel finite element methods are proposed. In Section 5, the theoretical analysis is presented. Some numerical results are reported to verify the validity and efficiency of the presented algorithms in Section 6. Finally, a conclusion is derived in Section 7.

2. The Stokes–Darcy Model

Let $\Omega_f \subset R^d (d = 2, 3)$ be a fluid region and $\Omega_p \subset R^d$ be a porous media region with $\Omega_f \cap \Omega_p = \emptyset$, $\overline{\Omega_f} \cap \overline{\Omega_p} = \Gamma$, $\overline{\Omega_f} \cup \overline{\Omega_p} = \overline{\Omega}$. Denote $\Gamma_f = \partial\Omega_f \backslash \Gamma$, $\Gamma_p = \partial\Omega_p \backslash \Gamma$.

In the fluid region Ω_f, the fluid is governed by the Stokes equations as follows:

$$\begin{cases} -\nabla \cdot \mathbb{T}(\boldsymbol{u}, p) = \boldsymbol{f}_1 & \text{in } \Omega_f, \\ \nabla \cdot \boldsymbol{u} = 0 & \text{in } \Omega_f, \end{cases} \tag{1}$$

where $\mathbb{T} = -p\mathbb{I} + 2\nu\mathbb{D}(\boldsymbol{u})$ is the stress tensor, $\mathbb{I}$ is the identity matrix, ν is the kinematic viscosity, $\mathbb{D}(\boldsymbol{u}) = \frac{1}{2}(\nabla \boldsymbol{u} + \nabla^T \boldsymbol{u})$ is the velocity deformation tensor, $\boldsymbol{u}$ represents the velocity, p represents the kinematic pressure, and $\boldsymbol{f}_1$ represents the external force.

In the porous media region Ω_p, the fluid is governed by the equations as follows:

$$\begin{cases} \nabla \cdot \boldsymbol{u}_p = f_2 & \text{in } \Omega_p, \\ \boldsymbol{u}_p = -\mathbb{K}\nabla\phi & \text{in } \Omega_p, \end{cases} \tag{2}$$

where $\boldsymbol{u}_p$ denotes the fluid velocity, f_2 denotes a source term, $\mathbb{K}$ denotes the hydraulic conductivity, and $\phi = z + \frac{p_p}{\rho g}$ denotes the piezometric head, with z being the height from a reference level, p_p being the dynamic pressure, ρ being the density of the fluid, and g being the gravitational acceleration.

Then, Equation (2) is rewritten in the following formalization:

$$-\nabla \cdot (\mathbb{K}\nabla\phi) = f_2 \qquad\qquad \text{in } \Omega_p, \tag{3}$$

which we shall consider in the following paper.

On the interface Γ, the following conditions are considered:

$$\begin{cases} \boldsymbol{u} \cdot \boldsymbol{n}_f + \boldsymbol{u}_p \cdot \boldsymbol{n}_p = 0, \\ -[\mathbb{T}(\boldsymbol{u}, p) \cdot \boldsymbol{n}_f] \cdot \boldsymbol{n}_f = \rho g \phi, \\ -[\mathbb{T}(\boldsymbol{u}, p) \cdot \boldsymbol{n}_f] \cdot \boldsymbol{\tau}_i = \alpha \sqrt{\frac{\nu g}{tr(\mathbb{K})}} \boldsymbol{u} \cdot \boldsymbol{\tau}_i, \end{cases} \tag{4}$$

where $\boldsymbol{n}_f$ is the unit normal vector on Γ from Ω_f to Ω_p, $\boldsymbol{n}_p$ is the unit normal vector on Γ from Ω_p to Ω_f, $\{\boldsymbol{\tau}_i\}_{i=1}^{d-1}$ are the tangential unit vectors on Γ, and α is a positive constant, which is dependent on the property of the porous media region. The first equation is the mass conservation, the second one denotes the balance of normal forces, and the last one is the well-known Beavers–Joseph–Saffman interface condition, which is the simplification of the Beavers–Joseph interface condition.

For the sake of simplicity, the following Dirichlet boundary conditions are considered:

$$\boldsymbol{u} = 0 \qquad \text{on } \Gamma_f, \qquad\qquad \phi = 0 \qquad \text{on } \Gamma_p.$$

In the following, the standard Sobolev spaces and related norms are utilized. Furthermore, for a domain D, let $(\cdot,\cdot)_D$ stand for the usual L^2 inner product on D. To derive the weak formulation of the mixed Stokes–Darcy problem, the following spaces are introduced:

$$\begin{aligned} &H_f = \{\boldsymbol{v} \in H^1(\Omega_f)^d : \boldsymbol{v} = 0 \text{ on } \Gamma_f\}, \\ &H_p = \{\psi \in H^1(\Omega_p) : \psi = 0 \text{ on } \Gamma_p\}, \\ &Q = L^2(\Omega_f), \\ &W = H_f \times H_p, \\ &X = W \times Q. \end{aligned}$$

Then, the weak formulation of the coupled Stokes–Darcy model with the Beavers–Joseph–Saffman interface condition reads as follows: find $\overrightarrow{u} = (\boldsymbol{u}, \phi) \in W$, $p \in Q$, such that

$$\begin{cases} a(\overrightarrow{u}, \overrightarrow{v}) + b(\overrightarrow{v}, p) = (\overrightarrow{f}, \overrightarrow{v}) & \forall \overrightarrow{v} = (\boldsymbol{v}, \psi) \in W, \\ b(\overrightarrow{u}, q) = 0 & \forall q \in Q, \end{cases} \tag{5}$$

where

$$\begin{aligned} &a(\overrightarrow{u}, \overrightarrow{v}) = a_\Omega(\overrightarrow{u}, \overrightarrow{v}) + a_\Gamma(\overrightarrow{u}, \overrightarrow{v}) = a_f(\boldsymbol{u}, \boldsymbol{v}) + a_p(\phi, \psi) + a_\Gamma(\overrightarrow{u}, \overrightarrow{v}), \\ &a_f(\boldsymbol{u}, \boldsymbol{v}) = 2\nu(\mathbb{D}(\boldsymbol{u}), \mathbb{D}(\boldsymbol{v}))_{\Omega_f} + \alpha\sqrt{\frac{\nu g}{tr(\mathbb{K})}} \int_\Gamma P_\tau \boldsymbol{u} \cdot P_\tau \boldsymbol{v}, \quad P_\tau \boldsymbol{v} = \sum_{j=1}^{d-1} (\boldsymbol{v} \cdot \boldsymbol{\tau}_j)\boldsymbol{\tau}_j, \\ &a_p(\phi, \psi) = \rho g(\mathbb{K}\nabla\phi, \nabla\psi)_{\Omega_p}, \quad a_\Gamma(\overrightarrow{u}, \overrightarrow{v}) = \rho g \int_\Gamma (\phi \boldsymbol{v} - \psi \boldsymbol{u}) \cdot \boldsymbol{n}_f, \\ &b(\overrightarrow{v}, p) \equiv b(\boldsymbol{v}, p) = -(p, \nabla \cdot \boldsymbol{v})_{\Omega_f}, \quad (\overrightarrow{f}, \overrightarrow{v}) = (\boldsymbol{f}_1, \boldsymbol{v})_{\Omega_f} + \rho g(f_2, \psi)_{\Omega_p}. \end{aligned}$$

3. Stabilized Finite Element Approximation

Let τ_h be a regular triangulation of Ω. The triangles K_i $(i = 1, \cdots, M)$ satisfy $\overline{\Omega} = \overline{K_1} \cup \overline{K_2} \cup \cdots \cup \overline{K_M}$, $h = \max\limits_{K \in \tau_h} diam(K)$. Assume the triangulation $\tau_h(\Omega_f)$ is compatible with $\tau_h(\Omega_p)$ on the interface Γ. Define the following finite element spaces as

$$
\begin{aligned}
&H_{f,h} = \{\boldsymbol{v} \in H_f : \boldsymbol{v}|_K \in \mathbf{P}_1 \triangleq P_1^d, \forall K \in \tau_h(\Omega_f)\},\\
&H_{p,h} = \{\psi \in H_p : \psi|_K \in P_1, \forall K \in \tau_h(\Omega_p)\},\\
&Q_h = \{q \in Q : q|_K \in P_1, \forall K \in \tau_h(\Omega_f)\},\\
&W_h = H_{f,h} \times H_{p,h},\\
&X_h = W_h \times Q_h.
\end{aligned}
$$

It is well known that the above finite element spaces $H_{f,h} \times Q_h$ do not satisfy the discrete inf-sup condition. To derive a stable numerical solution, the following stabilization term is introduced:

$$G(p, q) = \lambda((I - \Pi)p, (I - \Pi)q), \tag{6}$$

where the stabilization parameter λ satisfies $0 < \lambda < 1$. For the local pressure projection $\Pi : L^2(\Omega) \to R$, $R \subset \Omega$, there holds

$$(p, q) = (\Pi p, q) \quad \forall p \in L^2(\Omega),\ q \in R, \tag{7}$$

$$\|\Pi p\|_0 \le c\|p\|_0 \quad \forall p \in L^2(\Omega), \tag{8}$$

$$|(I - \Pi)p| \le ch^m\|p\|_m \quad \forall p \in H^m(\Omega),\ m = 0, 1. \tag{9}$$

Define the discrete form of Equation (6) with two Gauss integrals

$$G(p_h, q_h) = \lambda \sum_{K \in K_h} \left\{ \int_{K,2} p_h q_h dx - \int_{K,1} p_h q_h dx \right\} \quad \forall p_h, q_h \in Q_h, \tag{10}$$

where $\int_{K,m} \cdot d\mathbf{x}$ denotes a Gauss integral over K, K is exact for polynomials of degree m, and $m = 1, 2$.

Under the above notations, the stabilized finite element method of Equation (5) reads as follows: find $(\overrightarrow{u_h}, p_h) = (\boldsymbol{u}_h, \phi_h, p_h) \in X_h$, such that

$$
\begin{cases}
a(\overrightarrow{u_h}, \overrightarrow{v_h}) + b(\overrightarrow{v_h}, p_h) = (\overrightarrow{f}, \overrightarrow{v_h}) & \forall \overrightarrow{v_h} = (\boldsymbol{v}_h, \psi_h) \in W_h,\\
b(\overrightarrow{u_h}, q_h) + G(p_h, q_h) = 0 & \forall q_h \in Q_h.
\end{cases} \tag{11}
$$

Then, recall some error estimates of the stabilized finite element method deduced by Li et al., in [29].

$$
\begin{aligned}
&\|\boldsymbol{u} - \boldsymbol{u}_h\|_1 + \|\phi - \phi_h\|_1 + \|p - p_h\|_0 \le ch(\|\boldsymbol{u}\|_2 + \|\phi\|_2 + \|p\|_1),\\
&\|\boldsymbol{u} - \boldsymbol{u}_h\|_0 + \|\phi - \phi_h\|_0 \le ch^2(\|\boldsymbol{u}\|_2 + \|\phi\|_2 + \|p\|_1).
\end{aligned} \tag{12}
$$

Since $0 < \lambda < 1$, the above estimates still hold for Equation (11).

Then, the Stokes equation can be rewritten as

$$\mathscr{B}_s((\boldsymbol{u}_h, p_h); (\boldsymbol{v}_h, q_h)) = (\boldsymbol{f}_1, \boldsymbol{v}_h), \tag{13}$$

where

$$\mathscr{B}_s((\boldsymbol{u}_h, p_h); (\boldsymbol{v}_h, q_h)) = a_f(\boldsymbol{u}_h, \boldsymbol{v}_h) + b(\boldsymbol{v}_h, p_h) - b(\boldsymbol{u}_h, q_h) - G(p_h, q_h). \tag{14}$$

It is easy to verify that

$$|\mathscr{B}_s((\boldsymbol{u},p);(\boldsymbol{v},q))| \le c|||(\boldsymbol{u},p)|||_{\Omega_f}|||(\boldsymbol{v},q)|||_{\Omega_f}, \tag{15}$$

$$\beta|||(\boldsymbol{u}_h,p_h)|||_{\Omega_f} \le \sup_{(\boldsymbol{v}_h,q_h)\in H_{f,h}\times Q_h} \frac{|\mathscr{B}_s((\boldsymbol{u}_h,p_h);(\boldsymbol{v}_h,q_h))|}{|||(\boldsymbol{v}_h,q_h)|||_{\Omega_f}} \qquad \forall(\boldsymbol{u}_h,p_h)\in H_{f,h}\times Q_h, \tag{16}$$

where $|||(\boldsymbol{u}_h,p_h)|||_{\Omega_f} = \|\boldsymbol{u}_h\|_{1,\Omega_f} + \|p_h\|_{0,\Omega_f}$.

4. Numerical Algorithm

Divide Ω_f into a series of disjoint sub-domains D_j, and then enlarge D_j to Ω_j such that $D_j \subset\subset \Omega_j \subset\subset \Omega_f$ ($D_j \subset\subset \Omega_j$ means that $\mathrm{dist}(\partial D_j\backslash\partial\Omega_f, \partial\Omega_j\backslash\partial\Omega_f) > 0$). Define $\Gamma_{\Omega_j} = \Gamma\cap\partial\Omega_j$. Furthermore, divide Ω_p into a series of disjoint sub-domains D^i, then enlarge D^i to Ω^i. Then, obtain $D^i \subset\subset \Omega^i \subset\subset \Omega_p$ and define $\Gamma_{\Omega^i} = \Gamma\cap\partial\Omega^i$ similarly.

Algorithm 1 Local and parallel stabilized finite element method

Step 1. On a coarse grid, solve the following coupled model to find $(\overrightarrow{u_H}, p_H) \in X_H$ satisfying

$$\begin{cases} a(\overrightarrow{u_H},\overrightarrow{v_H}) + b(\overrightarrow{v_H},p_H) = (\overrightarrow{f},\overrightarrow{v_H}) & \forall\,\overrightarrow{v_H} = (\boldsymbol{v}_H,\psi_h)\in W_H, \\ b(\overrightarrow{u_H},q_H) + G(p_H,q_H) = 0 & \forall\, q_H\in Q_H. \end{cases} \tag{17}$$

Step 2. On a fine mesh, solve a series of local Darcy sub-problems in parallel as follows: Find the local residuals $\epsilon_h^i \in H_{p,h}(\Omega^i)$ ($i = 1,2,\cdots,M_p$, $h < H$) satisfying

$$a_p(\epsilon_h^i,\psi_h) = \rho g(f_2,\psi_h)_{\Omega^i} - a_p(\phi_H,\psi_h) + \rho g\int_{\Gamma_{\Omega^i}} \psi_h\boldsymbol{u}_H\cdot\boldsymbol{n}_f \quad \forall\psi_h\in H_{p,h}(\Omega^i), \tag{18}$$

and we set $\phi^h = \phi_H + \epsilon_h^i$ in D^i.
On a fine mesh, solve the following local Stokes sub-problems in parallel. Find local residuals $(\boldsymbol{e}_h^j,\eta_h^j) \in H_{f,h}(\Omega_j)\times Q_h(\Omega_j)$ ($j = 1,2,\cdots,M_f$), such that, for all $(\boldsymbol{v}_h,q_h) \in H_{f,h}(\Omega_j)\times Q_h(\Omega_j)$,

$$\begin{aligned} &a_f(\boldsymbol{e}_h^j,\boldsymbol{v}_h) + b(\boldsymbol{v}_h,\eta_h^j) = (\boldsymbol{f}_1,\boldsymbol{v}_h)_{\Omega_j} - (a_f(\boldsymbol{u}_H,\boldsymbol{v}_h) + b(\boldsymbol{v}_h,p_H)) - \rho g\int_{\Gamma_{\Omega_j}} \phi_H\boldsymbol{v}_h\cdot\boldsymbol{n}_f, \\ &b(\boldsymbol{e}_h^j,q_h) + G(\eta_h^j,q_h) = -b(\boldsymbol{u}_H,q_h) - G(p_H,q_h), \end{aligned} \tag{19}$$

and then set $(\boldsymbol{u}^h,p^h) = (\boldsymbol{u}_H + \boldsymbol{e}_h^j, p_H + \eta_h^j)$ in D_j.

However, the solution of the coupled Stokes–Darcy model Equation (11) derived by Algorithm 1 is globally discontinuous. By combining the local and parallel finite element method and the partition of unity method, a new local and parallel finite element method is obtained. Let $\{\Omega_f^j\}_{j=1}^{M_f}$ be an open cover of Ω_f and $\{\phi_j^f\}_{j=1}^{M_f}$ be the partition of unity subordinate to $\{\Omega_f^j\}_{j=1}^{M_f}$. Let $\{\Omega_p^i\}_{i=1}^{M_p}$ be an open cover of Ω_p and $\{\delta_i^p\}_{i=1}^{M_p}$ be the partition of unity subordinate to $\{\Omega_p^i\}_{i=1}^{M_p}$. ϕ_j^f and δ_i^p could be chosen as piecewise linear Lagrange basis functions. Then, there holds the following results [31]:

$$\begin{aligned}
\text{supp } \phi_j^f \subset \bar{\Omega}_f^j \quad & \forall j = 1, \cdots, M_f, \\
\sum_{j=1}^{M_f} \phi_j^f = 1 \qquad & \text{on } \Omega_f, \\
\|\phi_j^f\|_{L^\infty(R^d)} \leq c, & \\
\text{supp } \delta_i^p \subset \bar{\Omega}_p^i \quad & \forall i = 1, \cdots, M_p, \\
\sum_{i=1}^{M_p} \delta_i^p = 1 \qquad & \text{on } \Omega_p, \\
\|\delta_i^p\|_{L^\infty(R^d)} \leq c. &
\end{aligned}$$

Furthermore, construct the partition of unity as follows: Define a regular triangulation τ_{H_p} in Ω such that $h < H \leq H_p$, where H_p is fixed and independent of h, H. For the triangulation τ_{H_p}, let D_f^j be the union of triangles in Ω_f, and let D_p^i be the union of triangles in Ω_p. Define $\Gamma_{\Omega_f^j} = \Gamma \cap \partial\Omega_f^j$, $\Gamma_{\Omega_p^i} = \Gamma \cap \partial\Omega_p^i$.

Algorithm 2 Local and parallel partition of unity stabilized finite element method

Step 1. On a coarse grid, solve the following coupled model to obtain $(\overrightarrow{u_H}, p_H) \in X_H$, such that

$$\begin{cases} a(\overrightarrow{u_H}, \overrightarrow{v_H}) + b(\overrightarrow{v_H}, p_H) = (\overrightarrow{f}, \overrightarrow{v_H}) & \forall \overrightarrow{v_H} = (\boldsymbol{v}_H, \psi_h) \in W_H, \\ b(\overrightarrow{u_H}, q_H) + G(p_H, q_H) = 0 & \forall q_H \in Q_H. \end{cases} \tag{20}$$

Step 2. On a fine mesh, find local fine grid correction $\epsilon_h^i \in H_{p,h}(\Omega_p^i)$ $(i = 1, 2, \cdots, M_p$, $h < H)$, such that for all $\psi_h \in H_{p,h}(\Omega_p^i)$,

$$a_p(\epsilon_h^i, \psi_h) = \rho g(f_2, \psi_h)_{\Omega_p^i} - a_p(\phi_H, \psi_h) + \rho g \int_{\Gamma_{\Omega_p^i}} \psi_h \boldsymbol{u}_H \cdot \boldsymbol{n}_f, \tag{21}$$

and then assemble them together to derive a continuous solution as

$$\phi_H^h = \phi_H + \sum_{i=1}^{M_p} \delta_i^p \epsilon_h^i. \tag{22}$$

On a fine mesh, find the local corrections $(\boldsymbol{e}_h^j, \eta_h^j) \in H_{f,h}(\Omega_f^j) \times Q_h(\Omega_f^j)$ $(j = 1, 2, \cdots, M_f)$, $\forall(\boldsymbol{v}_h, q_h) \in H_{f,h}(\Omega_f^j) \times Q_h(\Omega_f^j)$ such that

$$\begin{aligned}
& a_f(\boldsymbol{e}_h^j, \boldsymbol{v}_h) + b(\boldsymbol{v}_h, \eta_h^j) = (\boldsymbol{f}_1, \boldsymbol{v}_h)_{\Omega_f^j} - (a_f(\boldsymbol{u}_H, \boldsymbol{v}_h) + b(\boldsymbol{v}_h, p_H)) - \rho g \int_{\Gamma_{\Omega_f^j}} \phi_H \boldsymbol{v}_h \cdot \boldsymbol{n}_f, \\
& b(\boldsymbol{e}_h^j, q_h) + G(\eta_h^j, q_h) = -b(\boldsymbol{u}_H, q_h) - G(p_H, q_h),
\end{aligned} \tag{23}$$

and then obtain the final approximation as

$$(\boldsymbol{u}_H^h, p_H^h) = (\boldsymbol{u}_H + \sum_{j=1}^{M_f} \phi_j^f \boldsymbol{e}_h^j, p_H + \sum_{j=1}^{M_f} \phi_j^f \eta_h^j). \tag{24}$$

5. Theoretical Analysis

In this section, the error estimates of the proposed algorithms are derived. Firstly, a lemma, which is crucial for the later analysis, is introduced. Then, the main results based upon the provided lemma are derived. The proof of the following lemma is similar to lemma 3.2 in [26] and so it will be omitted.

Lemma 1. *Let $D \subset\subset \Omega_0 \subset \Omega_f$, for $\boldsymbol{f} \in L^2(\Gamma_{\Omega_0})$, and $\lambda = \mathcal{O}(h)$, if there exists $(\boldsymbol{w}_h, r_h) \in H_{f,h} \times Q_h$ such that*

$$a_f(\boldsymbol{w}_h, \boldsymbol{v}_h) + b(\boldsymbol{v}_h, r_h) - b(\boldsymbol{w}_h, q_h) - G(r_h, q_h) = (\boldsymbol{f}, \boldsymbol{v}_h), \quad \forall(\boldsymbol{v}_h, q_h) \in H_{f,h}(\Omega_0) \times Q_h(\Omega_0),$$

then there holds

$$\|\boldsymbol{w}_h\|_{1,D} + \|r_h\|_{0,D} \le c(\|\boldsymbol{w}_h\|_{0,\Omega_0} + \|r_h\|_{-1,\Omega_0} + \|\boldsymbol{f}\|_{L^2(\Gamma_{\Omega_0})}). \tag{25}$$

Theorem 1. *Assume that Lemma 1 holds, $(\boldsymbol{u}, \phi, p)$ is the exact solution of (5), $(\boldsymbol{u}_h, \phi_h, p_h)$ is the solution of the standard finite element method, and $(\boldsymbol{u}^h, \phi^h, p^h)$ is the solution of Algorithm 1. The following estimates hold:*

$$\|\phi_h - \phi^h\|_{1,D^i} \le cH^2, \tag{26}$$

$$\|\boldsymbol{u}_h - \boldsymbol{u}^h\|_{1,D_j} + \|p_h - p^h\|_{0,D_j} \le cH^2. \tag{27}$$

Consequently, there holds

$$\|\phi - \phi^h\|_{1,D^i} \le c(h + H^2), \tag{28}$$

$$\|\boldsymbol{u} - \boldsymbol{u}^h\|_{1,D_j} + \|p - p^h\|_{0,D_j} \le c(h + H^2). \tag{29}$$

Proof. Taking $(\boldsymbol{v}_h, \psi_h) = (0, \psi_h)$ into Equation (11) yields

$$a_p(\phi_h, \psi_h) = \rho g(f_2, \psi_h) + \rho g \int_\Gamma \psi_h \boldsymbol{u}_h \cdot \boldsymbol{n}_f. \tag{30}$$

Since

$$a_p(\phi^h, \psi_h) = \rho g(f_2, \psi_h) + \rho g \int_{\Gamma_{\Omega^i}} \psi_h \boldsymbol{u}_H \cdot \boldsymbol{n}_f, \tag{31}$$

and setting $\psi_h = \phi_h - \phi^h$, there holds

$$a_p(\phi_h - \phi^h, \phi_h - \phi^h) = \rho g \int_{\Gamma_{\Omega^i}} (\phi_h - \phi^h)(\boldsymbol{u}_h - \boldsymbol{u}_H) \cdot \boldsymbol{n}_f. \tag{32}$$

Then, the auxiliary problem similar to [6] is introduced as follows: find $\delta \in H^1(\Omega_f)$, such that

$$\begin{cases} -\Delta\delta = 0 & \text{in } \Omega_f, \\ \delta = \phi_h - \phi^h & \text{on } \Gamma_{\Omega^i}, \\ \delta = 0 & \text{on } \partial\Omega_f / \Gamma_{\Omega^i}. \end{cases}$$

Recalling the interpolation space $H_{00}^{1/2}(\Gamma_{\Omega^i}) = [L^2(\Gamma_{\Omega^i}), H_0^1(\Gamma_{\Omega^i})]_{1/2}$ presented in [32], it follows that

$$\|\delta\|_{1,\Omega_f} \le c\|\phi_h - \phi^h\|_{H_{00}^{1/2}(\Gamma_{\Omega^i})} \le c\|\phi_h - \phi^h\|_{1,\Omega^i}. \tag{33}$$

Combining Equation (11) with Equation (17) yields

$$b(\boldsymbol{u}_h - \boldsymbol{u}_H, q_H) + G(p_h - p_H, q_H) = 0. \tag{34}$$

Hence,

$$\begin{aligned}
&\rho g \int_{\Gamma_{\Omega^i}} (\phi_h - \phi^h)(\boldsymbol{u}_h - \boldsymbol{u}_H) \cdot \boldsymbol{n}_f \\
&= \rho g \int_{\partial\Omega_f} \delta(\boldsymbol{u}_h - \boldsymbol{u}_H) \cdot \boldsymbol{n}_f \\
&= \rho g \int_{\Omega_f} \nabla\delta \cdot (\boldsymbol{u}_h - \boldsymbol{u}_H) + \rho g \int_{\Omega_f} \delta\nabla \cdot (\boldsymbol{u}_h - \boldsymbol{u}_H) \\
&= \rho g \int_{\Omega_f} \nabla\delta \cdot (\boldsymbol{u}_h - \boldsymbol{u}_H) + \rho g \int_{\Omega_f} (\delta - q_H)\nabla \cdot (\boldsymbol{u}_h - \boldsymbol{u}_H) + \rho g G(p_h - p_H, q_H).
\end{aligned} \tag{35}$$

Noting that Equation (12) holds, therefore, for $\delta \in H^1(\Omega_f)$, it can be derived that

$$\begin{aligned}
\|\phi_h - \phi^h\|^2_{1,\Omega^i} &= a_p(\phi_h - \phi^h, \phi_h - \phi^h) \\
&\leq c\|\delta\|_{1,\Omega_f}\|\boldsymbol{u}_h - \boldsymbol{u}_H\|_{0,\Omega_f} + c \inf_{\forall q_H \in Q_H} \left| \int_{\Omega_f} (\delta - q_H)\nabla \cdot (\boldsymbol{u}_h - \boldsymbol{u}_H) \right| \\
&\quad + cG(p_h - p_H, q_H - \delta) + cG(p_h - p_H, \delta) \\
&\leq cH^2\|\delta\|_{1,\Omega_f} + c \inf_{\forall q_H \in Q_H} \|\delta - q_H\|_{0,\Omega_f}\|\boldsymbol{u}_h - \boldsymbol{u}_H\|_{1,\Omega_f} \\
&\quad + c\|p_h - p_H\|_{0,\Omega_f} \inf_{\forall q_H \in Q_H} \|q_H - \delta\|_{0,\Omega_f} + c\|p_h - p_H\|_{0,\Omega_f}\|(I - \Pi)\delta\|_{0,\Omega_f} \\
&\leq cH^2\|\delta\|_{1,\Omega_f} \\
&\leq cH^2\|\phi_h - \phi^h\|_{1,\Omega^i}.
\end{aligned} \tag{36}$$

Then, Equation (26) is established.

Analogously, an auxiliary problem in the porous media domain is introduced: find $\Phi \in H^1(\Omega_p)$ such that

$$\begin{cases}
-\nabla \cdot (\mathbb{K}\nabla\Phi) = 0 & \text{in } \Omega_p, \\
\mathbb{K}\nabla\Phi \cdot \boldsymbol{n}_p = \rho g \boldsymbol{v}_h \cdot \boldsymbol{n}_p & \text{on } \Gamma_{\Omega_j}, \\
\mathbb{K}\nabla\Phi \cdot \boldsymbol{n}_p = 0 & \text{on } \partial\Omega_p/\Gamma_{\Omega_j}.
\end{cases}$$

It is classical that

$$\|\mathbb{K}^{1/2}\nabla\Phi\|_{0,\Omega_p} \leq c\|\boldsymbol{v}_h\|_{1,\Omega_j}, \tag{37}$$

and

$$\|\Phi\|_{2,\Omega_p} \leq c\|\boldsymbol{v}_h\|_{1,\Omega_j}. \tag{38}$$

Taking $(\boldsymbol{v}_h, \psi_h, q_h) = (\boldsymbol{v}_h, 0, q_h)$ into Equation (11) yields

$$a_f(\boldsymbol{u}_h, \boldsymbol{v}_h) + b(\boldsymbol{v}_h, p_h) - b(\boldsymbol{u}_h, q_h) - G(p_h, q_h) = (\boldsymbol{f}_1, \boldsymbol{v}_h) - \rho g \int_\Gamma \phi_h \boldsymbol{v}_h \cdot \boldsymbol{n}_f. \tag{39}$$

Subtracting Equation (19) from Equation (39) yields

$$\begin{aligned} &a_f(\boldsymbol{u}_h - \boldsymbol{u}^h, \boldsymbol{v}_h) + b(\boldsymbol{v}_h, p_h - p^h) - b(\boldsymbol{u}_h - \boldsymbol{u}^h, q_h) - G(p_h - p^h, q_h) \\ &\qquad + \rho g \int_{\Gamma_{\Omega_j}} (\phi_h - \phi_H)\boldsymbol{v}_h \cdot \boldsymbol{n}_f = 0 \qquad \forall(\boldsymbol{v}_h, q_h) \in H_{f,h}(\Omega_j) \times Q_h(\Omega_j). \end{aligned} \tag{40}$$

Using Lemma 1, it follows that

$$\begin{aligned} &\|\boldsymbol{u}_h - \boldsymbol{u}^h\|_{1,D_j} + \|p_h - p^h\|_{0,D_j} \\ &\leq c\left(\|\boldsymbol{u}_h - \boldsymbol{u}^h\|_{0,\Omega_j} + \|p_h - p^h\|_{-1,\Omega_j} + \frac{|\rho g \int_{\Gamma_{\Omega_j}} (\phi_h - \phi_H)\boldsymbol{v}_h \cdot \boldsymbol{n}_f|}{\|\boldsymbol{v}_h\|_{1,\Omega_j}} \right) \\ &\leq c\left(\|\boldsymbol{u}_h - \boldsymbol{u}_H\|_{0,\Omega_j} + \|\boldsymbol{u}_H - \boldsymbol{u}_h\|_{0,\Omega_j} + \|p_h - p_H\|_{-1,\Omega_j} + \|p_H - p^h\|_{-1,\Omega_j} + \frac{|\rho g \int_{\Gamma_{\Omega_j}} (\phi_h - \phi_H)\boldsymbol{v}_h \cdot \boldsymbol{n}_f|}{\|\boldsymbol{v}_h\|_{1,\Omega_j}} \right) \\ &= c\left(\|\boldsymbol{u}_h - \boldsymbol{u}_H\|_{0,\Omega_j} + \|p_h - p_H\|_{-1,\Omega_j} + \|\boldsymbol{e}_h^j\|_{0,\Omega_j} + \|\eta_h^j\|_{-1,\Omega_j} + \frac{|\rho g \int_{\Gamma_{\Omega_j}} (\phi_h - \phi_H)\boldsymbol{v}_h \cdot \boldsymbol{n}_f|}{\|\boldsymbol{v}_h\|_{1,\Omega_j}} \right). \end{aligned} \tag{41}$$

Now, estimate the last term on the right side of the above inequality. Following the idea in [33], there holds

$$\begin{aligned} \rho g \int_{\Gamma_{\Omega_j}} (\phi_h - \phi_H)\boldsymbol{v}_h \cdot \boldsymbol{n}_f &= -\int_{\Gamma_{\Omega_j}} (\phi_h - \phi_H)\mathbb{K}\nabla\Phi \cdot \boldsymbol{n}_p \\ &= -\int_{\partial\Omega_p} (\phi_h - \phi_H)\mathbb{K}\nabla\Phi \cdot \boldsymbol{n}_p \\ &= -\int_{\Omega_p} (\phi_h - \phi_H)\nabla \cdot (\mathbb{K}\nabla\Phi) - \int_{\Omega_p} \mathbb{K}\nabla \cdot (\phi_h - \phi_H) \cdot \nabla\Phi \\ &= -\int_{\Omega_p} \mathbb{K}\nabla \cdot (\phi_h - \phi_H) \cdot \nabla\Phi \\ &= -\int_{\Omega_p} \mathbb{K}\nabla \cdot (\phi_h - \phi^h) \cdot \nabla\Phi - \int_{\Omega_p} \mathbb{K}\nabla \cdot (\phi^h - \phi_H) \cdot \nabla\Phi. \end{aligned} \tag{42}$$

For the first term on the right side of the above inequality, it can be derived that

$$\left| -\int_{\Omega_p} \mathbb{K}\nabla \cdot (\phi_h - \phi^h) \cdot \nabla\Phi \right| \leq c\|\phi_h - \phi^h\|_{1,\Omega^i}\|\mathbb{K}^{1/2}\nabla\Phi\|_{0,\Omega_p} \leq cH^2\|\boldsymbol{v}_h\|_{1,\Omega_j}. \tag{43}$$

From Equation (11), it is easy to obtain

$$a_p(\phi^h, \psi_H) = \rho g(f_2, \psi_H) + \rho g \int_{\Gamma_{\Omega_j}} \psi_H \boldsymbol{u}_H \cdot \boldsymbol{n}_f. \tag{44}$$

Taking $(\boldsymbol{v}_H, \psi_H) = (0, \psi_H)$ into Equation (11) and using Equation (44) yields

$$-\int_{\Omega_p} \mathbb{K}\nabla \cdot (\phi^h - \phi_H) \cdot \nabla\psi_H = 0. \tag{45}$$

Hence,

$$\begin{aligned}\left|-\int_{\Omega_p}\mathbb{K}\nabla\cdot(\phi^h-\phi_H)\cdot\nabla\Phi\right| &= \left|-\int_{\Omega_p}\mathbb{K}\nabla\cdot(\phi^h-\phi_H)\cdot\nabla(\Phi-\psi_H)\right| \\ &\leq c\|\phi^h-\phi_H\|_{1,\Omega_p}\inf_{\forall\psi_H\in H_{p,H}}\|\Phi-\psi_H\|_{1,\Omega_p} \\ &\leq cH(\|\phi^h-\phi_h\|_{1,\Omega_p}+\|\phi_h-\phi_H\|_{1,\Omega_p})\|\Phi\|_{2,\Omega_p} \\ &\leq cH^2\|\boldsymbol{v}_h\|_{1,\Omega_j}. \end{aligned} \tag{46}$$

By using the above inequalities, it can be derived that

$$\left|\rho g\int_{\Gamma_{\Omega_j}}(\phi_h-\phi_H)\boldsymbol{v}_h\cdot\boldsymbol{n}_f\right| \leq cH^2\|\boldsymbol{v}_h\|_{1,\Omega_j}. \tag{47}$$

Next, a dual problem is introduced to estimate $\|\boldsymbol{e}_h^j\|_{0,\Omega_j}$ and $\|\eta_h^j\|_{-1,\Omega_j}$. For $\boldsymbol{\theta}\in L^2(\Omega_j)^d$, $\varphi\in H_0^1(\Omega_j)$, find $(\boldsymbol{w},r)\in(H_f(\Omega_j)\cap H^2(\Omega_j)^d)\times L^2(\Omega_j)$ such that for all $(\boldsymbol{v},q)\in H_f(\Omega_j)\times L^2(\Omega_j)$,

$$a_f(\boldsymbol{v},\boldsymbol{w})+b(\boldsymbol{w},q)-b(\boldsymbol{v},r)-G(q,r)=(\boldsymbol{\theta},\boldsymbol{v})_{\Omega_j}+(\varphi,q)_{\Omega_j}. \tag{48}$$

And there holds

$$\|\boldsymbol{w}\|_{2,\Omega_j}+\|r\|_{1,\Omega_j}\leq c(\|\boldsymbol{\theta}\|_{0,\Omega_j}+\|\varphi\|_{1,\Omega_j}). \tag{49}$$

Assume $(\boldsymbol{w}_\mu,r_\mu)\in H_{f,\mu}(\Omega_j)\times Q_\mu(\Omega_j)$ is derived by using the stabilized finite element method; then, there holds

$$a_f(\boldsymbol{v},\boldsymbol{w}-\boldsymbol{w}_\mu)+b(\boldsymbol{w}-\boldsymbol{w}_\mu,q)-b(\boldsymbol{v},r-r_\mu)-G(q,r-r_\mu)=0\quad\forall(\boldsymbol{v},q)\in H_{f,\mu}(\Omega_j)\times Q_\mu(\Omega_j), \tag{50}$$

where $\mu=h$ or H.

Apparently,

$$\begin{aligned}\|\boldsymbol{w}-\boldsymbol{w}_\mu\|_{1,\Omega_j}+\|r-r_\mu\|_{0,\Omega_j} &\leq c\mu(\|\boldsymbol{w}\|_{2,\Omega_j}+\|r\|_{1,\Omega_j}) \\ &\leq c\mu(\|\boldsymbol{\theta}\|_{0,\Omega_j}+\|\varphi\|_{1,\Omega_j}).\end{aligned} \tag{51}$$

Then, there holds

$$\|\boldsymbol{w}_h-\boldsymbol{w}_H\|_{1,\Omega_j}+\|r_h-r_H\|_{0,\Omega_j}\leq cH(\|\boldsymbol{\theta}\|_{0,\Omega_j}+\|\varphi\|_{1,\Omega_j}). \tag{52}$$

From Equation (17), it is easy to obtain

$$\begin{aligned}&a_f(\boldsymbol{u}_h-\boldsymbol{u}_H,\boldsymbol{w}_H)+b(\boldsymbol{w}_H,p_h-p_H)-b(\boldsymbol{u}_h-\boldsymbol{u}_H,r_H)-G(p_h-p_H,r_H) \\ &\quad+\rho g\int_{\Gamma_{\Omega_j}}(\phi_h-\phi_H)\boldsymbol{w}_H\cdot\boldsymbol{n}_f=0\qquad\forall(\boldsymbol{w}_H,r_H)\in H_{f,H}(\Omega_j)\times Q_H(\Omega_j).\end{aligned} \tag{53}$$

Taking $\boldsymbol{v}=\boldsymbol{e}_h^j$, $q=\eta_h^j$ into Equation (48), and together with Equations (40), (50), and (53) yields

$$
\begin{aligned}
&(\boldsymbol{\theta}, \boldsymbol{e}_h^j)_{\Omega_j} + (\varphi, \eta_h^j)_{\Omega_j} \\
&= a_f(\boldsymbol{e}_h^j, \boldsymbol{w}) + b(\boldsymbol{w}, \eta_h^j) - b(\boldsymbol{e}_h^j, r) - G(\eta_h^j, r) \\
&= a_f(\boldsymbol{e}_h^j, \boldsymbol{w}_h) + b(\boldsymbol{w}_h, \eta_h^j) - b(\boldsymbol{e}_h^j, r_h) - G(\eta_h^j, r_h) \\
&= a_f(\boldsymbol{u}_h - \boldsymbol{u}_H, \boldsymbol{w}_h) + b(\boldsymbol{w}_h, p_h - p_H) - b(\boldsymbol{u}_h - \boldsymbol{u}_H, r_h) - G(p_h - p_H, r_h) + \rho g \int_{\Gamma_{\Omega_j}} (\phi_h - \phi_H) \boldsymbol{w}_h \cdot \boldsymbol{n}_f \\
&= a_f(\boldsymbol{u}_h - \boldsymbol{u}_H, \boldsymbol{w}_h - \boldsymbol{w}_H) + b(\boldsymbol{w}_h - \boldsymbol{w}_H, p_h - p_H) - b(\boldsymbol{u}_h - \boldsymbol{u}_H, r_h - r_H) - G(p_h - p_H, r_h - r_H) \\
&\quad + \rho g \int_{\Gamma_{\Omega_j}} (\phi_h - \phi_H) \cdot (\boldsymbol{w}_h - \boldsymbol{w}_H) \cdot \boldsymbol{n}_f.
\end{aligned}
\tag{54}
$$

Based on Equations (12) and (51), it is valid that

$$
\begin{aligned}
&\left| (\boldsymbol{\theta}, \boldsymbol{e}_h^j)_{\Omega_j} + (\varphi, \eta_h^j)_{\Omega_j} \right| \\
&\leq (\|\boldsymbol{u}_h - \boldsymbol{u}_H\|_{1,\Omega_f} + \|p_h - p_H\|_{0,\Omega_f} + \|\phi_h - \phi_H\|_{1,\Omega_p})(\|\boldsymbol{w}_h - \boldsymbol{w}_H\|_{1,\Omega_j} + \|r_h - r_H\|_{0,\Omega_j}) \\
&\leq cH(\|\boldsymbol{u}_h - \boldsymbol{u}_H\|_{1,\Omega_f} + \|p_h - p_H\|_{0,\Omega_f} + \|\phi_h - \phi_H\|_{1,\Omega_p})(\|\boldsymbol{\theta}\|_{0,\Omega_j} + \|\varphi\|_{1,\Omega_j}) \\
&\leq cH^2(\|\boldsymbol{\theta}\|_{0,\Omega_j} + \|\varphi\|_{1,\Omega_j}).
\end{aligned}
\tag{55}
$$

Consequently,

$$
\|\boldsymbol{e}_h^j\|_{0,\Omega_j} + \|\eta_h^j\|_{-1,\Omega_j} \leq cH^2. \tag{56}
$$

In the following, the estimate of $\|p_h - p_H\|_{-1,\Omega_j}$ is deduced. Setting $(\boldsymbol{v}, q) = (\boldsymbol{u}_h - \boldsymbol{u}_H, p_h - p_H)$ in Equation (48), together with Equations (47), (51), and (53), and using the fact that $\|\boldsymbol{w}_H\|_{1,\Omega_j} \leq \|\boldsymbol{w} - \boldsymbol{w}_H\|_{1,\Omega_j} + \|\boldsymbol{w}\|_{1,\Omega_j} \leq c\|\boldsymbol{w}\|_{2,\Omega_j}$, it is easy to obtain

$$
\begin{aligned}
&\left| (\boldsymbol{\theta}, \boldsymbol{u}_h - \boldsymbol{u}_H)_{\Omega_j} + (\varphi, p_h - p_H)_{\Omega_j} \right| \\
&= \left| a_f(\boldsymbol{u}_h - \boldsymbol{u}_H, \boldsymbol{w}) + b(\boldsymbol{w}, p_h - p_H) - b(\boldsymbol{u}_h - \boldsymbol{u}_H, r) - G(p_h - p_H, r) \right| \\
&= | a_f(\boldsymbol{u}_h - \boldsymbol{u}_H, \boldsymbol{w} - \boldsymbol{w}_H) + b(\boldsymbol{w} - \boldsymbol{w}_H, p_h - p_H) - b(\boldsymbol{u}_h - \boldsymbol{u}_H, r - r_H) \\
&\quad - G(p_h - p_H, r - r_H) - \rho g \int_{\Gamma_{\Omega_j}} (\phi_h - \phi_H) \boldsymbol{w}_H \cdot \boldsymbol{n}_f | \\
&\leq c(\|\boldsymbol{u}_h - \boldsymbol{u}_H\|_{1,\Omega_j} + \|p_h - p_H\|_{0,\Omega_j})(\|\boldsymbol{w} - \boldsymbol{w}_H\|_{1,\Omega_j} + \|r - r_H\|_{0,\Omega}) + cH^2 \|w_H\|_{1,\Omega_j} \\
&\leq cH^2(\|\boldsymbol{w}\|_{2,\Omega_j} + \|r\|_{1,\Omega_j}) \\
&\leq cH^2(\|\boldsymbol{\theta}\|_{0,\Omega_j} + \|\varphi\|_{1,\Omega_j}).
\end{aligned}
\tag{57}
$$

Hence,

$$
\|\boldsymbol{u}_h - \boldsymbol{u}_H\|_{0,\Omega_j} + \|p_h - p_H\|_{-1,\Omega_j} \leq cH^2. \tag{58}
$$

Therefore, together with Equations (41), (47), (56), and (58), (27) is derived. By combing the triangle inequality with Equations (26) and (27), Equations (28) and (29) could be directly derived. □

Define the following norm as follows:

$$\left|\left|\left|\boldsymbol{u}_h - \boldsymbol{u}^h\right|\right|\right|_{1,\Omega_f} = (\sum_{j=1}^{M_f} \|\boldsymbol{u}_h - \boldsymbol{u}^h\|_{1,D_j})^{1/2},$$
$$\left|\left|\left|p_h - p^h\right|\right|\right|_{0,\Omega_f} = (\sum_{j=1}^{M_f} \|p_h - p^h\|_{0,D_j})^{1/2},$$
$$\left|\left|\left|\phi_h - \phi^h\right|\right|\right|_{1,\Omega_p} = (\sum_{i=1}^{M_p} \|\phi_h - \phi^h\|_{1,D^i})^{1/2}.$$

Then, the following theoretical results can be derived directly:

Theorem 2. *Based on Theorem 1, there holds*

$$\left|\left|\left|\boldsymbol{u}_h - \boldsymbol{u}^h\right|\right|\right|_{1,\Omega_f} + \|p_h - p^h\|_{0,\Omega_f} + \left|\left|\left|\phi_h - \phi^h\right|\right|\right|_{1,\Omega_p} \le cH^2. \tag{59}$$

Proof. By collecting the sub-domains D_j (D^i), $j = 1, \cdots, M_f$, $i = 1, \cdots, M_p$, the proof is finished. □

Theorem 3. *Assume that the condition of Theorem 2 holds, then for the solutions using Algorithm 2, there holds the following estimate:*

$$\|\boldsymbol{u}_h - \boldsymbol{u}_H^h\|_{1,\Omega_f} + \|p_h - p_H^h\|_{0,\Omega_f} + \|\phi_h - \phi_H^h\|_{1,\Omega_p} \le cH^2. \tag{60}$$

Proof. Since $\boldsymbol{u}_\mu = \sum_{j=1}^{M_f} \phi_j^f \boldsymbol{u}_\mu$, $p_\mu = \sum_{j=1}^{M_f} \phi_j^f p_\mu$, $\phi_\mu = \sum_{i=1}^{M_p} \delta_i^p \phi_\mu$, $\mu = h, H$, it is easy to obtain that

$$\begin{aligned}
&\|\boldsymbol{u}_h - \boldsymbol{u}_H^h\|_{1,\Omega_f} + \|p_h - p_H^h\|_{0,\Omega_f} + \|\phi_h - \phi_H^h\|_{1,\Omega_p} \\
&= \|\boldsymbol{u}_h - (\boldsymbol{u}_H + \sum_{j=1}^{M_f} \phi_j^f \boldsymbol{e}_h^j)\|_{1,\Omega_f} + \|p_h - (p_H + \sum_{j=1}^{M_f} \phi_j^f \eta_h^j)\|_{0,\Omega_f} + \|\phi_h - (\phi_H + \sum_{i=1}^{M_p} \delta_i^p \epsilon_h^i)\|_{1,\Omega_p} \\
&= \|\sum_{j=1}^{M_f} \phi_j^f (\boldsymbol{u}_h - \boldsymbol{u}_H - \boldsymbol{e}_h^j)\|_{1,\Omega_f} + \|\sum_{j=1}^{M_f} \phi_j^f (p_h - p_H - \eta_h^j)\|_{0,\Omega_f} + \|\sum_{i=1}^{M_p} \delta_i^p (\phi_h - \phi_H - \epsilon_h^i)\|_{1,\Omega_p} \\
&\le \sum_{j=1}^{M_f} \|\phi_j^f (\boldsymbol{u}_h - \boldsymbol{u}^h)\|_{1,D_f^j} + \sum_{j=1}^{M_f} \|\phi_j^f (p_h - p^h)\|_{0,D_f^j} + \sum_{i=1}^{M_p} \|\delta_i^p (\phi_h - \phi^h)\|_{1,D_p^i} \\
&\le \sum_{j=1}^{M_f} \|\phi_j^f\|_{L^\infty(\Omega_f)} \|\boldsymbol{u}_h - \boldsymbol{u}^h\|_{1,D_f^j} + \sum_{j=1}^{M_f} \|\phi_j^f\|_{L^\infty(\Omega_f)} \|p_h - p^h\|_{0,D_f^j} + \sum_{i=1}^{M_p} \|\delta_i^p\|_{L^\infty(\Omega_p)} \|\phi_h - \phi^h\|_{1,D_p^i} \\
&\le c \sum_{j=1}^{M_f} (\|\boldsymbol{u}_h - \boldsymbol{u}^h\|_{1,D_f^j} + \|p_h - p^h\|_{0,D_f^j}) + c \sum_{i=1}^{M_p} \|\phi_h - \phi^h\|_{1,D_p^i} \\
&\le cH^2.
\end{aligned} \tag{61}$$

□

6. Numerical Results

In this section, two examples are provided to verify the theoretical results and the efficiency and effectiveness of the proposed two parallel algorithms. The first test is a convergence test with a manufactured solution. The second one is a modification of a classical lid-driven cavity flow problem. Since it is difficult to directly solve the coupled scheme (11) as the mesh size tends to 0, we compared our algorithms with two parallel algorithms with $\mathbf{P}_1\mathbf{b}$-P_1-P_1 finite element pairs presented in [18]. We list some abbreviations and symbols in the following.

- **LPFEM—**Local and parallel finite element method with $\mathbf{P}_1\mathbf{b}$-P_1-P_1 finite element pairs;
- **LPPUFEM—**Local and parallel partition of unity finite element method with $\mathbf{P}_1\mathbf{b}$-P_1-P_1 finite element pairs;
- **LPSFEM—**Local and parallel stabilized finite element method;
- **LPPUSFEM—**Local and parallel partition of unity stabilized finite element method;
- $(\tilde{\mathbf{u}}^h, p^h, \phi^h)$—Solution obtained by **LPFEM**;
- $(\tilde{\mathbf{u}}_H^h, p_H^h, \phi_H^h)$—Solution obtained by **LPPUFEM**;
- $(\mathbf{u}^h, p^h, \phi^h)$—Solution obtained by **LPSFEM**;
- $(\mathbf{u}_H^h, p_H^h, \phi_H^h)$—Solution obtained by **LPPUSFEM**;
- $\mathcal{X}_\kappa$—Implement the method $\mathcal{X}$ by dividing the domain Ω_f and Ω_p into $\kappa = L \times L$ sub-domains.

6.1. Test 1

In this test, one example with the analytical solution was considered to test the convergence order. Let $\Omega_f = [0,1] \times [1,2]$, $\Omega_p = [0,1] \times [0,1]$, and $\Gamma = [0,1] \times \{1\}$. The exact solution is

$$\begin{cases} u_1 = (1-2x)(y-1), \\ u_2 = x(x-1) + (y-1)^2, \\ p = x(1-x)(y-1) + \frac{y^3}{3} - y^2 + y - 0.5, \\ \phi = x(1-x)(y-1) + \frac{y^3}{3} - y^2 + y - 0.5, \end{cases}$$

Then, f_1, f_2 can be derived by Equations (1) and (2), respectively. It is easy to verify that the solution satisfies the Beavers–Joseph–Saffman interface condition. For simplicity, let $\alpha, \nu, g, \rho = 1$, $\mathbb{K} = \mathbb{I}$.

In the following, we introduce the details for the decomposition of Ω_f and Ω_p with $\kappa = 2 \times 2$ sub-domains. In the flow domain, divide Ω_f into four disjoint sub-regions

$$D_1 = (0, 0.5) \times (1, 1.5) \qquad D_2 = (0.5, 1) \times (1, 1.5),$$
$$D_3 = (0, 0.5) \times (1.5, 2) \qquad D_4 = (0.5, 1) \times (1.5, 2),$$

and then enlarge them into

$$\Omega_1 = (0, 0.75) \times (1, 1.75) \qquad \Omega_2 = (0.25, 1) \times (1, 1.75),$$
$$\Omega_3 = (0, 0.75) \times (1.25, 2) \qquad \Omega_4 = (0.25, 1) \times (1.25, 2).$$

In the porous media flow domain, divide Ω_p into four disjoint sub-regions

$$D^1 = (0, 0.5) \times (0, 0.5) \qquad D^2 = (0.5, 1) \times (0, 0.5),$$
$$D^3 = (0, 0.5) \times (0.5, 1) \qquad D^4 = (0.5, 1) \times (0.5, 1),$$

and then enlarge them into

$$\Omega^1 = (0, 0.75) \times (0, 0.75) \qquad \Omega^2 = (0.25, 1) \times (0, 0.75),$$
$$\Omega^3 = (0, 0.75) \times (0.25, 1) \qquad \Omega^4 = (0.25, 1) \times (0.25, 1).$$

Let us introduce the process to construct partition of unity functions for the fluid region. Let $H_{fix} = 1/8$, and generate the uniform mesh triangulation $T_{H_{fix}}(\Omega_f)$. Let

$nd(nd = 81)$ represent the number of nodes, $bf[i]$ stand for the piecewise linear basis function defined on the node i, and the first function is generated as follows:

$$\phi_1^f = \bigcup_{i \in G} bf[i], \quad G = \{1 \leq i \leq 36 \text{ and } 1 \leq \{i \bmod 9\} \leq 4.\}$$

The other three functions could be obtained in the same way. We plot them in Figure 1 along with partition of unity functions for the porous media region.

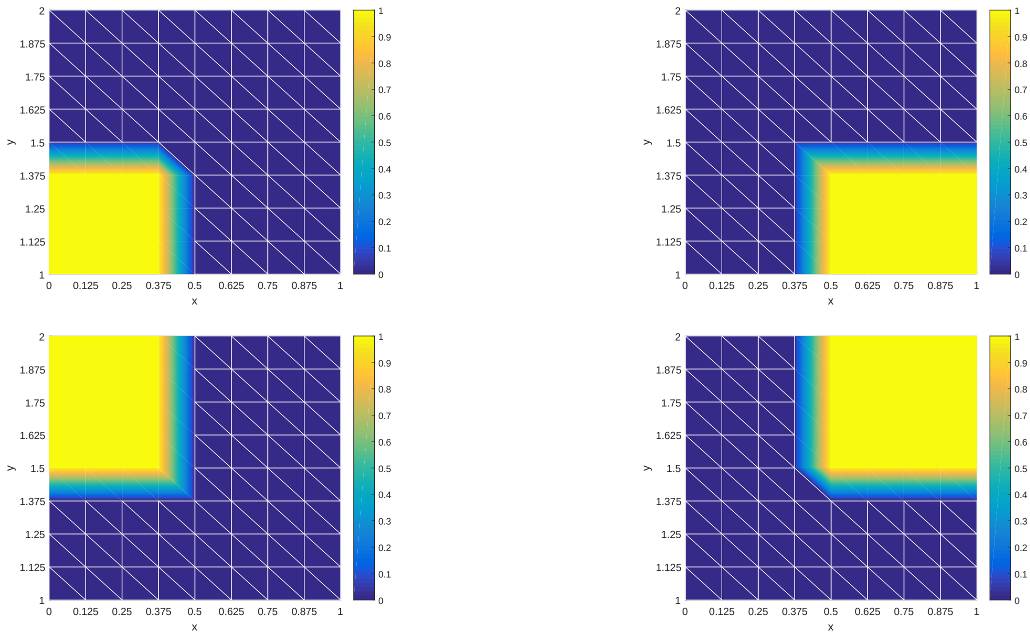

Figure 1. The partition of unity functions for the Stokes region.

The configuration between the coarse grid and the fine grid is $h = H^2$. In this case, the optimal error convergence rates of the proposed two algorithms could be derived. The uniform mesh is used, and the choice of λ is λ = 50 h.

The numerical results, including errors of the velocity, pressure, and piezometric head, obtained using four numerical methods are presented in Tables 1–6. As seen from these tables, we could derive the following conclusions:

(a) Convergence orders (for the velocity, pressure, and piezometric head) of the four algorithm are all one with respect to the fine mesh size h, which agrees with the theoretical results;

(b) **LPSFEM** derives a better approximation than **LPFEM** since the errors of **LPSFEM** are less than that of **LPFEM**. The same conclusion is suitable for the comparison of **LPPUSFEM** and **LPPUFEM**;

(c) **LPSFEM** and **LPPUSFEM** exhibit almost the same errors, which indicates that the partition of unity functions scarcely ever affect the error accuracy. The same situation happens to **LPFEM** and **LPPUFEM**.

Table 1. The H^1-error of the velocity of **LPSFEM**$_{2\times2}$, **LPFEM**$_{2\times2}$.

$\mathbf{1/H}$	$\mathbf{1/h}$	$\left\|\left\|\left\| u - u^h \right\|\right\|\right\|_{1,\Omega_f}$	*Rate*	$\left\|\left\|\left\| u - \tilde{u}^h \right\|\right\|\right\|_{1,\Omega_f}$	*Rate*
4	16	7.48065×10^{-2}	–	1.11563×10^{-1}	–
8	64	1.79323×10^{-2}	1.03030	2.65643×10^{-2}	1.03515
12	144	8.01801×10^{-3}	0.99258	1.18060×10^{-2}	1.00004

Table 2. The L^2-error of the pressure of $\mathbf{LPSFEM}_{2\times2}$, $\mathbf{LPFEM}_{2\times2}$.

1/H	**1/h**	$\left\|\left\|\left\|p - p^h\right\|\right\|\right\|_{0,\Omega_f}$	*Rate*	$\left\|\left\|\left\|p - \tilde{p}^h\right\|\right\|\right\|_{0,\Omega_f}$	*Rate*
4	16	5.32697×10^{-3}	–	2.38948×10^{-2}	–
8	64	1.05020×10^{-3}	1.17133	4.58095×10^{-3}	1.19149
12	144	4.42233×10^{-4}	1.06655	2.14858×10^{-3}	0.93361

Table 3. The H^1-error of the piezometric head of $\mathbf{LPSFEM}_{2\times2}$, $\mathbf{LPFEM}_{2\times2}$.

1/H	**1/h**	$\left\|\left\|\left\|\phi - \phi^h\right\|\right\|\right\|_{1,\Omega_p}$	*Rate*	$\left\|\left\|\left\|\phi - \tilde{\phi}^h\right\|\right\|\right\|_{1,\Omega_p}$	*Rate*
4	16	3.88154×10^{-2}	–	3.88539×10^{-2}	–
8	64	9.29858×10^{-3}	1.03077	9.30783×10^{-3}	1.03077
12	144	4.11933×10^{-3}	1.00400	4.12162×10^{-3}	1.00454

Table 4. The H^1-error of the velocity of $\mathbf{LPPUSFEM}_{2\times2}$, $\mathbf{LPPUFEM}_{2\times2}$.

1/H	**1/h**	$\|\|u - u^h_H\|\|_{1,\Omega_f}$	*Rate*	$\|\|u - \tilde{u}^h_H\|\|_{1,\Omega_f}$	*Rate*
4	16	7.37754×10^{-2}	–	1.0415×10^{-1}	–
8	64	1.79583×10^{-2}	1.01924	2.5565×10^{-2}	1.01319
12	144	7.91917×10^{-3}	1.00966	1.1437×10^{-2}	0.99195

Table 5. The L^2-error of the pressure of $\mathbf{LPPUSFEM}_{2\times2}$, $\mathbf{LPPUFEM}_{2\times2}$.

1/H	**1/h**	$\|\|p - p^h_H\|\|_{0,\Omega_f}$	*Rate*	$\|\|p - \tilde{p}^h_H\|\|_{0,\Omega_f}$	*Rate*
4	16	4.25241×10^{-3}	–	2.45224×10^{-2}	–
8	64	9.77831×10^{-4}	1.06031	4.56773×10^{-3}	1.21228
12	144	4.18785×10^{-4}	1.04569	2.24674×10^{-3}	0.87496

Table 6. The H^1-error of the piezometric head of $\mathbf{LPPUSFEM}_{2\times2}$, $\mathbf{LPPUFEM}_{2\times2}$.

1/H	**1/h**	$\|\|\phi - \phi^h_H\|\|_{1,\Omega_p}$	*Rate*	$\|\|\phi - \tilde{\phi}^h_H\|\|_{1,\Omega_p}$	*Rate*
4	16	3.75083×10^{-2}	–	3.75503×10^{-2}	–
8	64	9.28420×10^{-3}	1.00718	9.29392×10^{-3}	1.00723
12	144	4.08802×10^{-3}	1.0115	4.09047×10^{-3}	1.01205

In Table 7, we show the computational time of the four algorithms. As observed from this table, it is clear that $\mathbf{LPSFEM}_{2\times2}$ and $\mathbf{LPPUSFEM}_{2\times2}$ take less time than $\mathbf{LPFEM}_{2\times2}$ and $\mathbf{LPPUFEM}_{2\times2}$, namely, the two algorithms presented in this paper are more efficient.

Table 7. The comparison of CPU time.

1/h	$\mathbf{LPSFEM}_{2\times2}$	$\mathbf{LPFEM}_{2\times2}$	$\mathbf{LPPUSFEM}_{2\times2}$	$\mathbf{LPPUFEM}_{2\times2}$
16	0.042	0.064	0.044	0.066
64	0.406	0.547	0.410	0.55
144	2.078	2.672	2.085	2.675
256	6.186	9.279	6.193	9.385
400	17.012	33.258	17.02	33.271

To show the relation between the computational accuracy and CPU time with numbers of sub-domains, we ran Algorithms 1 and 2 by dividing Ω_f (Ω_p) into 2×2, 3×3, and 4×4 sub-domains, respectively. The computing results and CPU time are plotted in Figure 2. It is not hard to see that the numerical results support the theoretical findings from Figure 2a–c.

Furthermore, as seen from Figure 2d, as the number of sub-domains increases, the CPU time decreases, which is in accordance with our expectation.

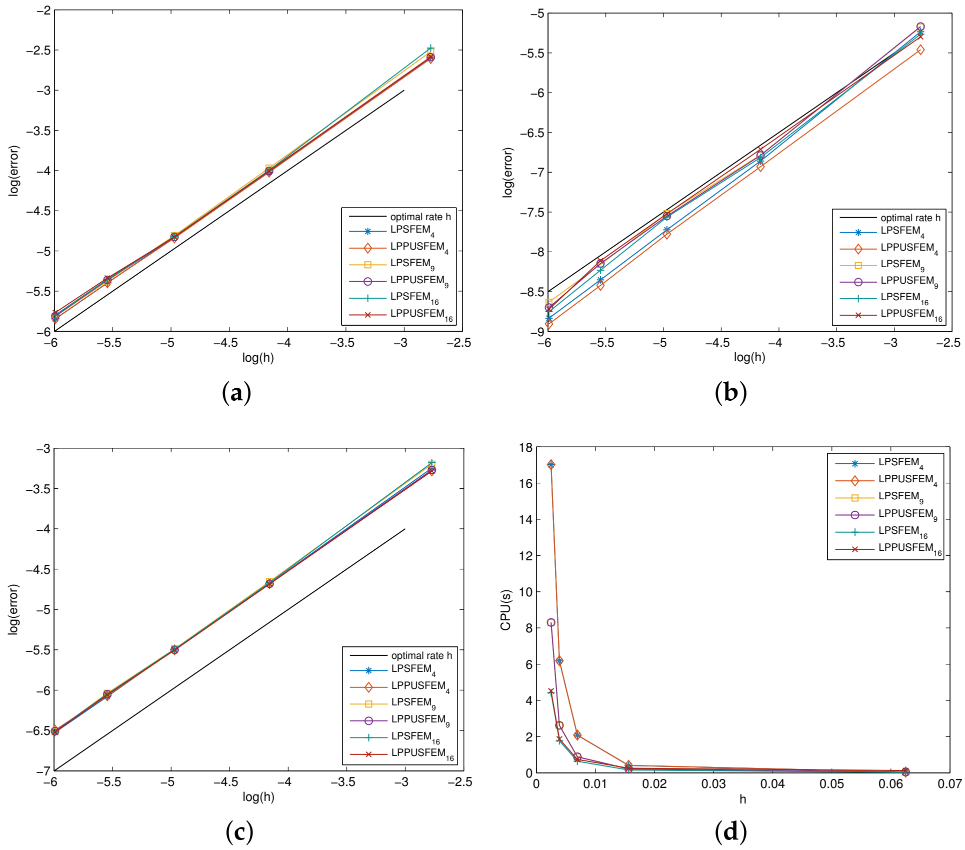

Figure 2. The performance of the solution using different algorithms: (**a**) velocity in H^1-norm; (**b**) pressure in L^2-norm; (**c**) piezometric head in H^1-norm (**d**) CPU time.

6.2. Test 2

In this test, the computational domain and physical parameters were chosen as in test 1. The following modified lid-driven cavity flow problem was considered

$$\mathbf{u}|_{\Gamma_f} = \begin{cases} (1,0), & (x,y) \in [0,1] \times \{2\}, \\ (0,0), & (x,y) \in \{0\} \times [1,2] \cup \{1\} \times [1,2], \end{cases} \tag{62}$$

and

$$\phi|_{\Gamma_p} = 0.$$

The external forces were set to 0, namely, $\mathbf{f}_1 = \mathbf{0}$ and $f_2 = 0$. The mesh sizes were chosen as $h = H^2 = (1/16)^2$. Since the exact solution is unknown, we plot out the streamlines of four algorithms in Figure 3 for a comparison. As observed from Figure 3, the four algorithms derived similar results.

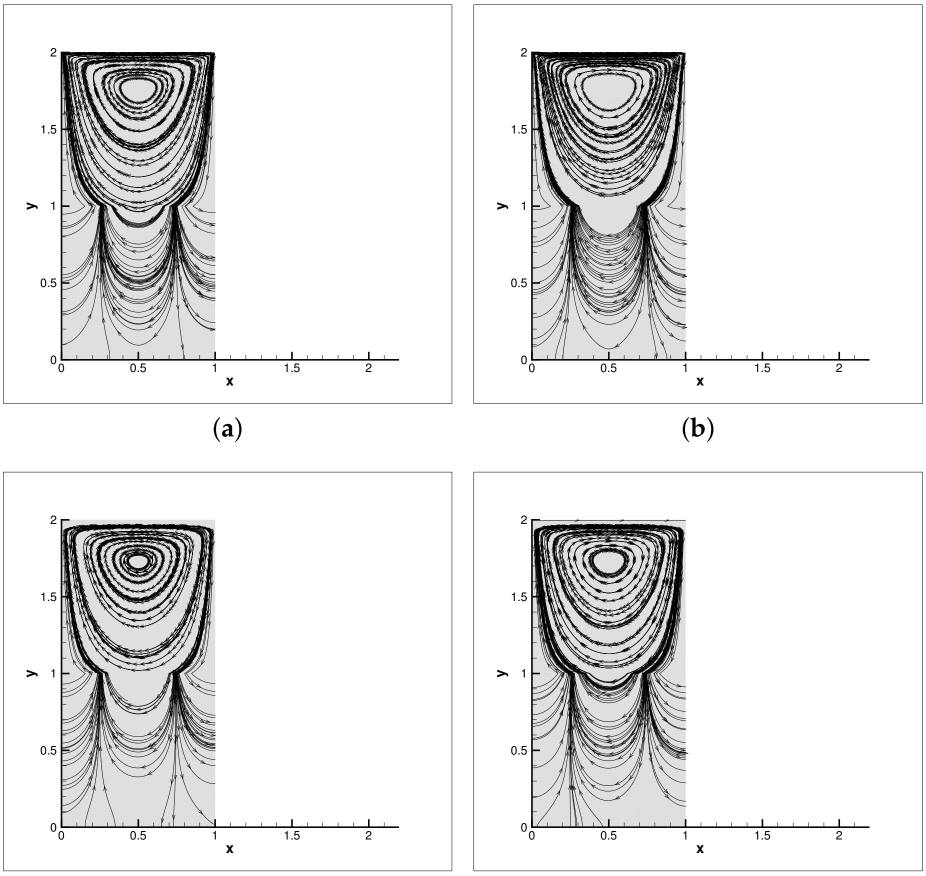

(**a**) (**b**)

(**c**) (**d**)

Figure 3. Streamlines of four algorithms: (**a**) streamline of $\mathbf{LPSFEM}_{2\times 2}$; (**b**) streamline of $\mathbf{LPPUSFEM}_{2\times 2}$; (**c**) streamline of $\mathbf{LPFEM}_{2\times 2}$; (**d**) streamline of $\mathbf{LPPUFEM}_{2\times 2}$.

7. Conclusions

In this study, by utilizing the two-grid decoupled technique and the overlapping domain decomposition method, two local and parallel stabilized finite element algorithms are proposed and investigated for the mixed Stokes–Darcy model using the lowest equal-order finite element pairs. The algorithms were devised to circumvent the inf-sup condition by offsetting the discrete pressure space using the residual of the simple and symmetry term at the element level. The theoretical results indicate that the two proposed algorithms could arrive at the same error accuracy and convergence rates with the one-level method by properly choosing the configuration between the two mesh sizes. Some numerical results are reported to verify the theoretical findings and illustrate the efficiency and robustness of the proposed two algorithms.

Author Contributions: Conceptualization, G.D.; Methodology, J.H.; Formal analysis, G.D.; Writing—original draft, J.H.; Writing—review & editing, G.D.; Visualization, J.H. All authors have read and agreed to the published version of the manuscript.

Funding: This work was subsidized by NSFC (Grant No. 12172202), the Support Plan for Outstanding Youth Innovation Team in Shandong Higher Education Institutions (No. 2022KJ249), the Natural Science Foundation of Shandong Province (Grant No. ZR2021MA063).

Data Availability Statement: Data are contained within the article.

Conflicts of Interest: The authors declare no conflict of interest.

References

1. Cao, Y.; Gunzburger, M.; Hu, X.; Hua, F.; Wang, X.; Zhao, W. Finite element approximation for Stokes-Darcy flow with Beavers-Joseph interface conditions. *SIAM J. Numer. Anal.* **2010**, *47*, 4239–4256. [CrossRef]
2. Rivire, B.; Yotov, I. Locally conservative coupling of Stokes and Darcy flows. *SIAM J. Numer. Anal.* **2005**, *42*, 1959–1977. [CrossRef]
3. Rui, H.; Zhang, R. A unified stabilized mixed finite element method for coupling Stokes and Darcy flows. *Comput. Methods Appl. Mech. Eng.* **2009**, *198*, 2692–2699. [CrossRef]
4. Cai, M.; Mu, M.; Xu, J. Numerical solution to a mixed Navier-Stokes/Darcy model by the two-grid approach. *SIAM J. Numer. Anal.* **2009**, *47*, 3325–3338. [CrossRef]
5. Du, G.; Zuo, L. A two-grid method with backtracking for the mixed Stokes/Darcy model. *J. Numer. Math.* **2021**, *29*, 39–46.
6. Mu, M.; Xu, J. A two-grid method of a mixed Stokes-Darcy model for coupling fluid flow with porous media flow. *SIAM J. Numer. Anal.* **2007**, *45*, 1801–1813. [CrossRef]
7. Cai, M.; Mu, M. A multilevel decoupled method for a mixed Stokes/Darcy model. *J. Comput. Appl. Math.* **2012**, *236*, 2452–2465. [CrossRef]
8. Chen, W.; Gunzburger, M.; Hua, F.; Wang, X. A parallel Robin-Robin domain decomposition method for the Stokes-Darcy system. *SIAM J. Numer. Anal.* **2011**, *49*, 1064–1084. [CrossRef]
9. He, X.; Li, J.; Lin, Y.; Ming, J. A domain decomposition method for the steady-state Navier-Stokes-Darcy model with the Beavers-Joseph interface condition. *SIAM J. Sci. Comput.* **2015**, *37*, S264–S290. [CrossRef]
10. Jiang, B. A parallel domain decomposition method for coupling of surface and groundwarter flows. *Comput. Methods Appl. Mech. Eng.* **2009**, *198*, 947–957. [CrossRef]
11. Sun, Y.; Sun, W.; Zheng, H. Domain decomposition method for the fully-mixed Stokes-Darcy coupled problem. *Comput. Methods Appl. Mech.* **2021**, *374*, 113578. [CrossRef]
12. Xu, J.; Zhou, A. Local and parallel finite element algorithms based on two-grid discretizations. *Math. Comput.* **2000**, *69*, 881–909. [CrossRef]
13. Xu, J.; Zhou, A. Local and parallel finite element algorithms based on two-grid discretizations for nonlinear problems. *Adv. Comput. Math.* **2001**, *14*, 293–327. [CrossRef]
14. He, Y.; Xu, J.; Zhou, A.; Li, J. Local and parallel finite element algorithms for the Stokes problem. *Numer. Math.* **2008**, *109*, 415–434. [CrossRef]
15. He, Y.; Xu, J.; Zhou, A. Local and parallel finite element algorithms for the Navier-Stokes problem. *J. Comput. Math.* **2006**, *24*, 227–238.
16. Shang, Y.; He, Y. Parallel iterative finite element algorithms based on full domain partition for the stationary Navier-Stokes equations. *Appl. Numer. Math.* **2010**, *60*, 719–737. [CrossRef]
17. Zheng, B.; Shang, Y. Local and parallel stabilized finite element algorithms based on the lowest equal-order elements for the steady Navier-Stokes equations. *Math. Comput. Simul.* **2020**, *178*, 464–484. [CrossRef]
18. Du, G.; Zuo, L. Local and parallel finite element methods for the coupled Stokes/Darcy model. *Numer. Algor.* **2021**, *87*, 1593–1611. [CrossRef]
19. Zuo, L.; Du, G. A parallel two-grid linearized method for the coupled Navier-Stokes-Darcy problem. *Numer. Algor.* **2018**, *77*, 151–165. [CrossRef]
20. Zhang, Y.; Hou, Y.; Shan, L.; Dong, X. Local and parallel finite element algorithm for stationary incompressible magnetohydrodynamics. *Numer. Methods Partial. Differ. Equ.* **2017**, *33*, 1513–1539. [CrossRef]
21. Du, G.; Zuo, L. A Parallel Partition of Unity Scheme Based on Two-Grid Discretizations for the Navier-Stokes Problem. *J. Sci. Comput.* **2018**, *75*, 1445–1462. [CrossRef]
22. Yu, J.; Shi, F.; Zheng, H. Local and parallel finite element algorithms based on the partition of unity for the stokes problem. *SIAM J. Sci. Comput.* **2014**, *36*, C547–C567. [CrossRef]
23. Song, L.; Gao, M. A posteriori error estimates for the stabilization of low-order mixed finite elements for the Stokes problem. *Comput. Methods Appl. Mech. Eng.* **2014**, *279*, 410–424. [CrossRef]
24. Dohrmann, C.; Bochev, P. A stabilized finite element method for the Stokes problem based on polynomial pressure projections. *Int. J. Numer. Meth. Fluids* **2004**, *46*, 183–201. [CrossRef]
25. He, Y.; Li, J. A stabilized finite element method based on local polynomial pressure projection for the stationary Navier-Stokes equations. *Appl. Numer. Math.* **2008**, *58*, 1503–1514. [CrossRef]
26. Shang, Y. A parallel stabilized finite element method based on the lowest equal-order elements for incompressible flows. *Computing* **2020**, *102*, 65–81. [CrossRef]
27. Li, J.; He, Y.; Chen, Z. A new stabilized finite element method for the transient Navier-Stokes equations. *Comput. Methods Appl. Mech. Eng.* **2007**, *197*, 22–35. [CrossRef]
28. Li, J.; He, Y. A stabilized finite element method based on two local Gauss integrations for the Stokes equations. *J. Comp. Appl. Math.* **2008**, *214*, 58–65. [CrossRef]
29. Li, R.; Li, J.; Chen, Z.; Gao, Y. A stabilized finite element method based on two local Gauss integrations for a coupled Stokes-Darcy problem. *J. Comput. Appl. Math.* **2016**, *292*, 92–104. [CrossRef]
30. Zheng, H.; Hou, Y.; Shi, F.; Song, L. A finite element variational multiscale method for incompressible flows based on two local Gauss integrations. *J. Comput. Phys.* **2009**, *228*, 5961–5977. [CrossRef]

31. Melenk, J.M.; Babuška, I. The Partition of Unity Finite Element Method: Basic Theory and Applications. *Comput. Meth. Appl. Mech. Eng.* **1996**, *139*, 289–314. [CrossRef]
32. Lions, J.L.; Magenes, E. *Non-Homogeneous Boundary Value Problems and Applications*; Springer: New York, NY, USA; Heidelberg, Germany, 1972; Volume 1.
33. Hou, Y. Optimal error estimates of a decoupled scheme based on two-grid finite element for mixed Stokes-Darcy model. *Appl. Math. Lett.* **2016**, *57*, 90–96. [CrossRef]

Disclaimer/Publisher's Note: The statements, opinions and data contained in all publications are solely those of the individual author(s) and contributor(s) and not of MDPI and/or the editor(s). MDPI and/or the editor(s) disclaim responsibility for any injury to people or property resulting from any ideas, methods, instructions or products referred to in the content.